Heliyon 10 (2024) e29333

Contents lists available at ScienceDirect

Heliyon

journal homepage: www.cell.com/heliyon

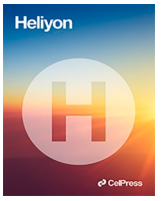

Research article

Harnessing HEK293 cell-derived exosomes for hsa-miR-365a-3p delivery: Potential application in hepatocellular carcinoma therapy

Armita Ghotaslou [a], Arezou Azizsoltani [a,b], Kaveh Baghaei [b,c,**], Effat Alizadeh [a,*]

[a] Department of Medical Biotechnology, Faculty of Advanced Medical Sciences, Tabriz University of Medical Sciences, Tabriz, Iran
[b] Basic and Molecular Epidemiology of Gastrointestinal Disorders Research Center, Research Institute for Gastroenterology and Liver Diseases, Shahid Beheshti University of Medical Sciences, Tehran, Iran
[c] Gastroenterology and Liver Diseases Research Center, Research Institute for Gastroenterology and Liver Diseases, Shahid Beheshti University of Medical Sciences, Tehran, Iran

ARTICLE INFO

Keywords:
MiR-365a-3p mimic
Cell cycle
ROS
Exosome
HepG2
Nrf2
HEK293

ABSTRACT

Hepatocellular carcinoma (HCC) is the most frequent form of liver malignancy, and curing it is very challenging. Restoring tumor suppressor microRNAs could trigger the initiation of cellular anticancer mechanisms. Exosomes are nanosized biocarriers capable of fusing with cell membranes and delivering their cargo. The main goal of the current study was to explore the potential of human embryonic kidney cells (HEK293) cell-derived exosomes to provide an anticancer therapy based on the restoration of tumor suppressor miR-365a downregulated in HepG2 cells. To accomplish this aim, exosomes were isolated from the HEK293 cell line culture and characterized, enriched by Homo sapiens (hsa) miR-365a-3p mimics. Exosomes enabled an efficient loading and intracellular delivery of hsa-miR-365a mimics, which translated into G0/G1 cell cycle arrest, induction of oxidative stress, reduction of migration capacity, and high apoptosis rate. The findings indicate that the delivery of miR-365a-3p by HEK293-derived exosomes may act as an innovative and effective therapeutic strategy against HCC.

1. Introduction

Hepatocellular carcinoma (HCC) is defined as a multi-stage malignancy of the liver [1] and ranked as the fifth most common and second most lethal cancer amongst all [2]. A recent transcriptome profiling study has documented alterations in microRNAs levels in HCC [3]. A great part of post-transcriptional tuning of gene expression is attributed to miRNAs, which are short (22-29 nt) riboregulators without being translated into any protein and contribute to almost all cellular phenomena. They were identified to be either downregulated (tumor suppressor role) or upregulated (oncogene function) during tumor initiation and progression [4]. Previous investigations have found that miR-365a-3p is repeatedly downregulated and acts as a tumor suppressor in some cancers [5].

The term oxidative stress refers to excessive levels of reactive oxygen species (ROS) which can trigger the development of various

* Corresponding author. Effat Alizadeh, PhD Department of Medical Biotechnology, Faculty of Advanced Medical Sciences, Tabriz University of Medical Sciences, Tabriz, Iran.
** Corresponding author. Kaveh Baghaei, PhDResearch Institute of Gastroenterology and Liver Disease (RIGLD), Aerabi St, Yemen St. Chamran Highway, Tehran, Iran.
E-mail addresses: Kavehbaghai@sbmu.ac.ir (K. Baghaei), alizadehe@tbzmed.ac.ir (E. Alizadeh).

https://doi.org/10.1016/j.heliyon.2024.e29333
Received 22 June 2023; Received in revised form 30 March 2024; Accepted 5 April 2024
Available online 9 April 2024

diseases [6]. Similar to other mechanisms in cancer cells, redox homeostasis is abnormal in HCC. While lower levels of ROS molecules may support tumorigenesis, elevated ROS levels can be lethal [7,8]. As the accelerated proliferation cycles are accompanied by assembly of higher ROS, they try to adapt themselves by increasing their antioxidant capacity to reduce ROS and prevent its amplification, which can induce senescence and apoptosis [9].

The nuclear factor-erythroid 2-related factor 2 (Nrf2) is considered a master regulator of cellular antioxidant response, which, under normal physiological conditions, is inactivated by binding to Kelch-like ECH-associated protein-1 (Keap1) [10]. Under oxidative and electrophilic stress conditions, however, Nrf2 is detached from Keap1, transported to nucleus, and dimerized with the small Maf protein (sMaf). The Nrf2-sMaf heterodimer binds to antioxidant response elements (ARE) in DNA and, along with other transcriptional activators, induces the transcription of cytoprotective genes [11]. Previous studies have shown that Nrf2-deficient mice are more prone to cancer than the wild type, indicating that Nrf2 has protective impacts on normal cells by quenching ROS [12]. Over-activation of Nrf2 induces growth, increases resistance to chemotherapy, and leads to metastasis through several mechanisms, including drug detoxification, prevention of drug accumulation via drug efflux transporters, suppression of apoptosis, and induction of angiogenesis [13]. In addition, Nrf2 over-expression is associated with poor prognoses and aggressive HCC phenotypes [11]. In general, the Nrf2/Keap1 pathway can be considered a signaling pathway actively involved in the progression and drug resistance of cancer. Thus, controlling this pathway can be a potential therapeutic strategy in malignancies. Several miRNAs have been reported to regulate the Nrf2 or oxidative stress pathway at several points [14]. The migration potential of breast cancer cells was significantly reduced by the inhibition of A Disintegrin and metalloproteinase 10 (ADAM10) [15]. Meanwhile, Up-regulated levels of ADAM10 in colon cancer cells leads to a malignant phenotype, promoting metastasis to the liver [16,17]. A study conducted by Hong et al. revealed that treatment with hsa-miR-365a-3p in colorectal cancer resulted in the suppression of ADAM10 and Jak/STAT signaling [18]. Thus, investigating the effects of hsa-miR-365a-3p delivery on ADAM10 expression in HCC could be beneficial for the development of new therapeutic approaches.

Identifying an efficient delivery system for miRNAs is still a challenge, because naked miRNA mimics are negatively charged and unable to efficiently penetrate cell membranes. Moreover, they are very vulnerable to RNase-mediated degradation [19].

Exosomes are 30–150 nm cell-derived microvesicles that facilitate intercellular communication by transporting nucleic acids, proteins, and lipids upon contact with target cell surfaces [20]. They play crucial roles in cellular functions like proliferation and apoptosis. These small vesicles, composed of nucleic acids, proteins, mRNA, lipids, and other biological substances, exhibit diverse functions based on their cellular origins [21,22]. Consequently, extensive research has explored the potential clinical applications of exosomes, including drug delivery systems [23], therapeutic carriers, and biomarkers [22]. Due to their natural origin and ability to traverse biological barriers, exosomes offer promising nano-sized carriers [24]. Among various cell sources, HEK293-derived exosomes are particularly advantageous due to their lack of cancer-related antigens, which could potentially stimulate the immune system, and the ease of transfection [25,26].

The present study investigated whether the exosome-mediated transient upregulation of miR-365a-3p mimics can initiate antitumor mechanisms on an HCC model cell line (HepG2).

2. Materials and methods

2.1. Cell lines

The HEK293 and HepG2 cell lines were purchased from the National Biological Resource Center (Tehran, Iran). Cells were cultured according to previously published protocol [27] and in 80 % confluency were washed with phosphate-buffered saline (PBS). The routine medium was replaced with serum-free medium (SFM).

2.2. Isolation and characterization of HEK293 cell-derived exosomes

When the cells were completely stabilized in SFM, the adapted cells were kept in the incubator at 37 °C, and after 48 h, the conditioned media (CM) were collected. Exosomes were extracted from CM using the Exocib kit (Cibzist, Tehran, Iran). Briefly, the CM was centrifuged (Eppendorf, Hamburg, Germany) at 300×*g* for 10 min to removed cell debris and dead cells. Then, the supernatant was filtered using a 0.22-μm filter. Next, the supernatant was mixed with reagent A at a 5:1 ratio. The mixture was vortexed thoroughly for 5 min and incubated for 12 h at 4 °C. Subsequently, the tubes were vortexed again for 1 min and then centrifuged for 40 min at 300×*g* at 4 °C. Finally, the supernatant was completely discarded, and the exosome pellet was resuspended in 50–200 μL of reagent B and stored at −80 °C.

2.2.1. Dynamic light scattering (DLS) and protein quantification

The size and polydispersity index (PDI) of the isolated exosomes were analyzed by NANOPHOX particle size analyzer (Sympatec, Germany), Additionally the protein concentration of exosomes was measured using a bicinchoninic acid (BCA) protein quantification kit (BCA, Thermo Scientific, Rockford, USA) as per the manufacturer's instructions.

2.2.2. Electron microscopy

Exosome size and morphology were analyzed using both field emission scanning electron microscopy (FE-SEM) and transmission electron microscopy (TEM). In FE-SEM imaging, the exosome suspension was dropped on a sterile glass substrate overnight at 25 °C to be dried and sputtered by gold for subsequent observation with an FE-SEM instrument (SEM, EM3200, KYKY, China). In TEM

examination, roughly a drop of isolated exosome was dried on 300-mesh formvar-carbon-coated copper grids for 5 min. The excess fluid was then carefully removed with filter paper and the grid negatively stained with 2 % (w/v) uranyl acetate for the next 3 min. Next, TEM analysis was performed (TEM, Carl Zeiss, Oberkochen, Germany).

2.2.3. Western blotting

Exosomal and cellular proteins were extracted with the RIPA lysis buffer containing Tris-HCL, EDTA, NaCl, sodium deoxycholate, SDS, protease inhibitor cocktail, and 1 % Triton NP40. The protein concentration was quantified by the Bradford method, and protein lysates were run on SDS-polyacrylamide gel. After electrophoresis, the separated protein bands were transferred to polyvinylidene difluoride (PVDF) membranes (Millipore, USA), which were subsequently blocked and washed. The blots were incubated for 16–18 h with primary antibodies CD9 (mouse monoclonal antibody, cat. No. sc-13118), CD63 (mouse monoclonal, cat. No.sc-5275), CD81 (mouse monoclonal, cat. No.sc-166029), Nrf2 (mouse monoclonal, cat. No.sc-365949), ADAM10 (mouse monoclonal antibody, cat. No. sc-365949), and β-Actin (mouse monoclonal antibody, cat. No.sc-47778) as internal controls (Santa Cruz Biotechnology, Inc., Dallas, USA). The secondary antibodies, mouse anti-rabbit IgG-HRP (mouse monoclonal, cat. No. sc-2357) at a dilution of 1:10000 (Santa Cruz Biotechnology, Inc., Dallas, USA), were added and incubated for 90 min at room temperature (RT). Eventually, blots were visualized by chemiluminescence (ECL) detection reagents (Sigma) [28].

2.3. Loading the exosomes with miR-365a-3p mimic

The FAM dye labeled-miR-365a-3p mimic was ordered and purchased from Bioneer (Korea). The modified calcium chloride method was used to load miR-365a-3p into the exosomes [29]. Initially, 150 pmol miR-365a-3p was mixed with 0.5 μg/ml exosomes in 150 μl PBS and 150 μl CaCl2 (0.1 M). Then, the mixture was placed on ice for 30 min, incubated for 60 s at 42 °C, and then incubated on ice for an additional 5 min. The final volume of the mixture was adjusted to 5 ml with PBS, and the exosomes were reisolated using the Exocib kit. Free unloaded miR-365a-3p was eliminated by incubating with 2 μg/ml RNase A (EN0531, Thermo Fisher) for 20 min at 37 °C. The activation of RNase A was stopped by adding 2 μg/ml RNase inhibitor (Thermo Fisher) and incubating for 15 min at 37 °C.

2.4. Quantification of miRNA loading into the exosome

A FAM dye-labeled miR-365a-3p was used to validate the entrance of miR into the exosomes. For this purpose, 15 μg of exosomes and exosomes-loaded miR-365a-3p mimic (ExomiR-365a-3p) were diluted in 2 ml PBS and analyzed by flow cytometry (MACSQuantAnalyser 10, Miltenyi Biotech, Germany) and FlowJo software. Moreover, the loading efficiency of the miR-365a-3p mimic in the exosomes was evaluated by real-time PCR in which miR-365a-3p expression was compared in unloaded and miR-loaded exosomes. Total miRNA was extracted using a miRNA isolation kit (Yekta Tajhiz Azama, Tehran, Iran) according to the manufacturer's instructions and stored at −80 °C. The synthesis of cDNA was conducted using a commercial kit (Yekta Tajhiz Azama, Iran). Next, miR-365a-3p expression levels were determined using an SYBR Green Master Mix Kit (Ampliqon, Odense, Denmark) and then normalized to U6 snRNA as an endogenous control. The $2^{-\Delta\Delta Ct}$ method was employed for analysis of the results.

2.5. Cellular uptake assay

2.5.1. Quantitative real-time PCR of miRNA expression

To analyze cellular uptake of ExomiR-365a-3p by the HepG2 cell line, cells were seeded in 6-well plates (5×10^5 cells per well) and allowed to adhere for 24 h. Then, the cells were treated with 14 μg/ml of ExomiR-365a-3p or exosomes at 37 °C for 24 h. After incubation, the cells were harvested to analyze the relative expression of miRNA by real-time PCR. In brief, total miRNA was isolated using miRNA isolation kit (Yekta Tajhiz Azama, Tehran, Iran) according to the manufacturer's instructions. To determine the expression of the miR-365a-3p mimic, miRNA was converted to complementary DNA from 200 ng total miRNA using stem loop RT-PCR method (Yekta Tajhiz Azama, Iran). The qPCR measurement was performed using the SYBR green master mix (Ampliqon, Herlev, Denmark). The amount of miR-365a-3p was normalized with the small nuclear RNA (snRNA) U6 as a housekeeping gene, and the fold change was calculated using the $2^{-\Delta\Delta Ct}$ comparative method. The sequences of the primers used were listed in Table 1.

2.5.2. Fluorescent microscopic/visualization of miRNA uptake in HepG2 cell line

Because this microRNA was labeled with FAM fluorescent dye at the 5′-end, it's presence could be visualized through green

Table 1
Primer sequences used for qRT-PCR.

Gene	Sequence
GAPDH	Fw: 5′-TTGCCCTCAACGACCACTTT -3′ Rev: 5′- TGGTCCAGGGGTCTTACTCC-3′
Bcl-2	Fw: 5′- ACTGGAGAGTGCTGAAGATTG-3′ Rev: 5′-GTCTACTTCCTCTGTGATGTTGT-3′
hsa-miR-365a-3p	Fw: 5′-ACACTATAGCTGGGTAATGCCCCTAAAA-3′ Universal reverse: 5′-TGGTGTCGTGGAGTCGGCAATTCAGTTG-3′
snRNA U6	Fw: 5′-ACACTTCCATCTGGGTCGTGAAGCGTTC-3′ Universal reverse: 5′-TGGTGTCGTGGAGTCGGCAATTCAGTTG-3′

fluorescence emission using Olympus inverted fluorescent microscopes. For this purpose, the cells were cultured in 6-well plates at a density of 25×10^4 cells/well. After 24 h of incubation, the cells were co-cultured with exosomes or 40 μg/ml ExomiR-365a-3p. Subsequently, after 24 h of co-culture, the emission of FAM-labeled green fluorescence was observed using an inverted fluorescent microscope and compared with the exosome-treated groups.

2.6. Cell cycle analysis

The HepG2 cells were seeded in 6-well plates and treated with various concentrations (3.5, 7, and 14 μg/ml) of ExomiR-365a-3p or free exosomes. After 48 h, the cells (10^6 cells/ml) were harvested using enzymatic digestion and centrifuged. The protocol was performed following the protocol described in previous reports [30]. Subsequently, the cells were analyzed using flow cytometry with Cell Quest software.

2.7. Cell apoptosis detection

Apoptosis detection in cells was conducted using the ApoFlowEx® fluorescein isothiocyanate (FITC) kit from Exbio (Vestec, Czech Republic) with flow cytometry. Briefly, HepG2 cells (2.5×10^5 cell/well) were cultured in 6-well plates for 24 h and then treated with different concentrations (3.5, 7, and 14 μg/ml) of ExomiR-365a-3p and exosomes for 48 h. The control group remained untreated. After the treatment period, both the treated and untreated groups were harvested with trypsin, and after centrifugation, the cell suspensions were stained with 5 μl annexin V–fluorescein isothiocyanate (FITC) and 5 μl propidium iodide (PI) (ApoFlowEx® FITC kit), according to the manufacturer's protocol, the stained cells were then incubated for 15 min at RT in darkness, and then analyzed by flow cytometry and Cell Quest software.

2.8. Real time PCR

To assess the expression level of the *Bcl-2* gene, the cells were treated with ExomiR-365a-3p and exosomes. After 48 h of treatment, total RNA was isolated using Super Trizol reagent (MX Cell, Tehran, Iran) according to the manufacturer's instructions and stored at −80 °C. The expression of the *Bcl-2* genes was evaluated using 1 μg of total RNA reverse-transcribed to cDNA with a cDNA synthesis kit (Yekta Tajhiz Azama, Iran). The mRNA expression levels were quantified using the SYBR green master mix (Ampliqon, Herlev, Denmark). The expression levels of target genes after normalization to *GAPDH* as an internal control were calculated using the ΔΔCt method. The primers were designed using OLIGO 7 software (Molecular Biology Insights, Inc., USA). The primer sequences are provided in Table 1.

2.9. Immunocytochemistry (ICC) staining

Immunocytochemistry (ICC) staining was used to determine Nrf2 protein. For this purpose, the cells were seeded in 8-well chamber slides, incubated for 24 h, and then treated with different concentrations (3.5, 7, and 14 μg/ml) of ExomiR-365a-3p or exosomes for 48 h in 100 μl DMEM/F-12 with 10 % FBS medium. The cells were then fixed immediately with 4 % paraformaldehyde in PBS (pH 7.4) for 10 min at RT and permeabilized with PBS containing 0.1–0.25 % Triton X-100 for 10 min. Following washing, the cells were blocked with 1 % BSA and subsequently incubated in the diluted primary antibody against Nrf2 (mouse monoclonal antibody cat. No. sc-365949) (Santa Cruz Biotechnology) in 1 % BSA for 1h at RT or overnight at 4 °C. After washing, cells were incubated with the secondary antibody (Goat Anti-Mouse IgG H&L (FITC) cat. No. ab6785) in 1 % BSA for 1 h at RT in the dark. For nuclei staining, cells were incubated with 4,6-diamidino-2-phenylindole (DAPII; Abcam) for 1 min at RT, washed, and finally visualized under an inverted fluorescence microscope.

2.10. ROS assay

In this experiment, 2′,7′-dichlorodihydrofluorescein diacetate (DCFDA) (Kiazist-Iran) was used to quantify ROS. The cells were treated with ExomiR-365a-3p or exosomes for 48 h and then harvested and resuspended in ROS buffer. Next, 15×10^5 cells were placed in duplicate microtube. After centrifuging the solution and removal of the supernatant, 100 μl of the working solution was added to each microtube and incubated at 37 °C for 45 min in a dark place. Following this the solution was discarded and the ROS buffer was added to each tube. The ROS concentration was assessed immediately by measuring excitation/emission absorbance at 485/535.

2.11. Wound healing assay

The HepG2 cells were seeded in 6-well plates (3×10^5 cells/well) and allowed to reach about 80 % confluence. Then, the media was removed and replaced with PBS. Subsequently, a tip was used to scratch the cell monolayer, and the PBS was moved gently to remove the detached cells. The media was exchanged with fresh media containing different concentrations of exosomes and ExomiR-365a-3p (14 μg/ml). The gaps were photographed 0, 12, 24, and 48 h after treatment using a live-cell imaging system (Olympus, Japan).

2.12. Statistical analysis

Statistical analysis was performed using GraphPad Prism software (version 9). Data were presented in the format of mean ± SD and analyzed using one-way analysis of variance (ANOVA) with Tukey post-hoc test between multiple groups. A value of $p \leq 0.05$ was considered statistically significant.

3. Results

3.1. Characterization of HEK293-derived exosomes

HEK293-derived exosomes were characterized by their morphology, size, and diameter of particles as well as the presence of exosomal surface markers. Based on the protein content of exosomes measured by BCA protein assay, the average yield of the exosomal protein was 1.8 μg/μl from 300 ml conditioned media. Morphology and size distribution of HEK293-derived exosomes were verified through SEM and TEM analysis, showing the presence of nearly spherical membrane particles with diameters ranging from 50 to 80 nm (Fig. 1 a-c). The size of exosomes was evaluated using DLS (NANOPHOX particle size analysis), and the average size of the exosomes was found to be 60 nm (Fig. 1d). The specific exosomal proteins (CD63, CD81, CD9) were confirmed by Western blot assay (Fig. 1e).

3.2. Validation of miR-365a-3p transfection into exosomes

The flow cytometry histogram revealed a significant fluorescent signal in the ExomiR-365a-3p mimic (81.3 %) group, indicating the efficiency of the loading of miR-365a-3p mimic in exosomes (Fig. 2a). In contrast, the free exosomes group did not exhibit any detectable signal. Moreover, the results of real-time PCR showed a significantly higher level of miR-365a-3p in ExomiR-365a-3p compared to the free exosome group (~4500-fold change, p-value< 0.0001) (Fig. 2b). These results confirm proper loading of miR-365a-3p in exosomes.

3.3. Efficient delivery of miR-365a-3p-loaded exosomes into HepG2 cell line

To evaluate if exosomes can efficiently act as bio-carriers for delivering miR-365a-3p mimics to target cells, we performed fluorescent microscopy and real-time PCR analysis. Fluorescent microscopy images confirmed the successful entry of FAM-labeled miRNAs into the HepG2 cell line after 24 h of incubation (Fig. 3a). In addition, the levels of miR-365a-3p in ExomiR-treated, exosome-treated, and untreated groups were analyzed using real-time PCR. The results revealed a significant difference between the ExomiR-365a-3p-treated groups and both the exosome-treated and untreated groups (p-value< 0.0001). However, no significant difference was

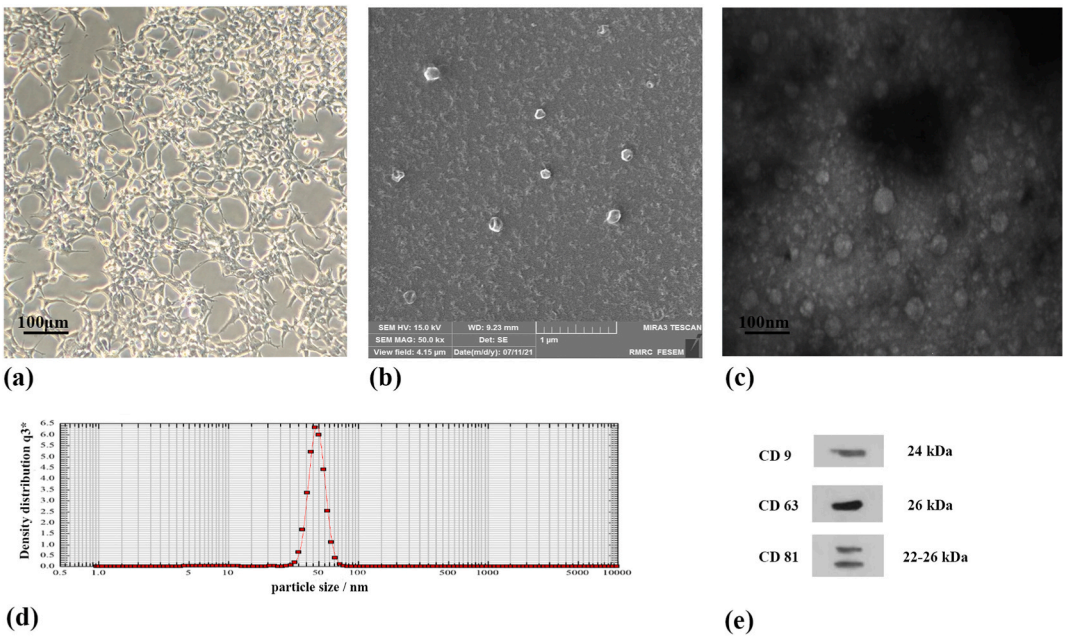

Fig. 1. Characterization of HEK293 cell-derived exosomes. (a) Microscopic image of HEK293 cultured for exosome isolation (10x). (b) FE-SEM image of HEK293 cell-originated exosomes. (c) TEM image of exosomes. (d) DLS detected size distribution of HEK293 isolated exosomes. (e) Western blot analysis verifies the expression of exosomal surface markers (CD9, CD63, CD81). The original gel blot is shown in Fig. 1e of the Supplementary file.

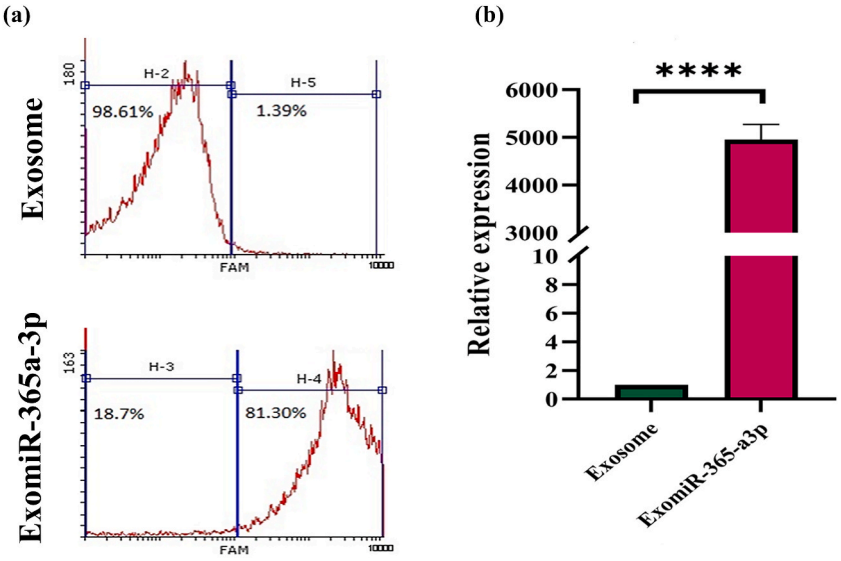

Fig. 2. Efficacy of loading miR-365a-3p into HEK293 isolated exosomes quantified by flow cytometry and real time-PCR. (a) Flow cytometry analysis of the relative fluorescence intensity showed high accumulation of miR-365a-3p in miR transfected groups. (b) The relative expression of miR-365a-3p determined by qRT-PCR (p-value <0.0001).

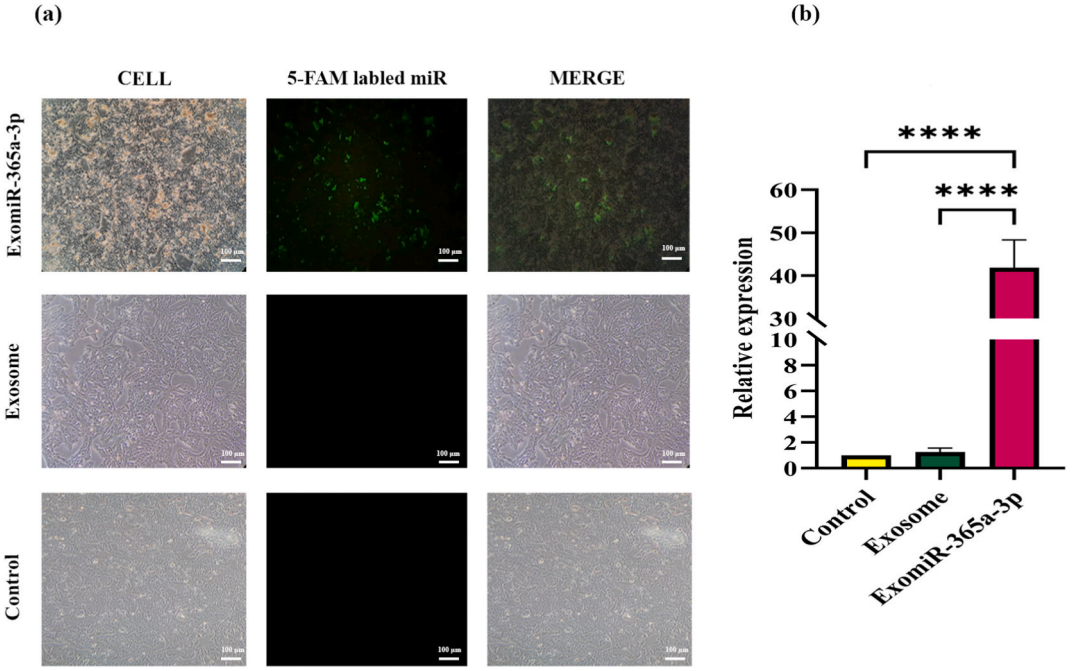

Fig. 3. The relative frequency of miR-365a-3p transcripts in HepG2 cell line treated with ExomiR-365a-3p and unloaded exosomes determined by fluorescence microscopy images and real time PCR. (a) Fluorescence microscopy images of HepG2 cells treated with ExomiR-365a-3p and exosomes. Green fluorescence emitted from HepG2 cells transfected by FAM-labeled ExomiR-365a-3p; magnification (4x). (b) Fold changes of miR-365a-3p levels in HepG2 cells treated by ExomiR-365a-3p and exosomes after 24 h incubation. U6 snRNA was used as an internal control. (The data are representative of three independent experiments presented as mean ± SD.****p-value <0.0001). (For interpretation of the references to color in this figure legend, the reader is referred to the Web version of this article.)

observed between the free exosome group and the untreated group (Fig. 3b).

3.4. miR-365a-3p-enriched exosomes induced apoptosis in HepG2cell line

The effect of delivering miR-365a-3p through exosomes on HepG2 cell apoptosis was carefully examined to clarify the functional role of miR-365a-3p in these cells. As shown in Fig. 4, ExomiR-365a-3p significantly increased cell apoptosis in a dose-dependent manner compared to the unloaded exosome groups (Fig. 4). Data analysis revealed no substantial difference in the amount of apoptosis between the untreated cells as a negative control and the exosome-treated cells. However, the apoptosis rate in the groups treated with 7 and 14 μg/ml ExomiR-365a-3p exhibited a remarkable increase compared to the groups treated with 7 and 14 μg/ml of free exosomes (p-value< 0.0001) after 48 h of treatment. Moreover, apoptosis in the group that received 14 μg/ml of ExomiR-365a-3p increased significantly in comparison with the cells that received 7 μg/ml of ExomiR-365a-3p (p-value<0.01), and both concentrations (7 and 14 μg/ml) had a considerable effect on apoptotic cell rate compared with 3.5 μg/ml ExomiR-365a-3p (p-value< 0.0001). The details of data are shown in the Supplementary figure.

3.5. Nrf2 protein level is negatively regulated by ExomiR-365a-3p

Fluorescence microscopy indicated reduction in Nrf2 protein expression in the ExomiR-365a-3p treated groups (Fig. 5a). Western blot analysis further confirmed a significant decrease in the Nrf2 protein level in the ExomiR-365a-3p treated groups (Fig. 5b and c).

3.6. ExomiR-365a-3p negatively affected HepG2 cell cycle

The HepG2 cells were transfected with various levels of ExomiR-365a-3p mimics and subsequently subjected to PI staining and flow cytometry analysis to assess cell cycle distribution. Treatment with HEK293-derived exosomes at different doses resulted in the accumulation of HepG2 cells in the G0/G1 phase of the cell cycle (Fig. 6). Similarly, exposure to ExomiR-365a-3p increased entry into the G0/G1 phase and augmented the sub-G peaks in the population presenting histograms. Therefore, ExomiR-365-3p disturbed the cell cycle and induced entrance into the apoptosis phase (sub G).

3.7. Treatment with ExomiR-365a-3p increases ROS and induces intrinsic pathway of apoptosis

Given that high levels of mitochondrial ROS can initiate the intrinsic apoptosis process, the cellular ROS levels were evaluated in

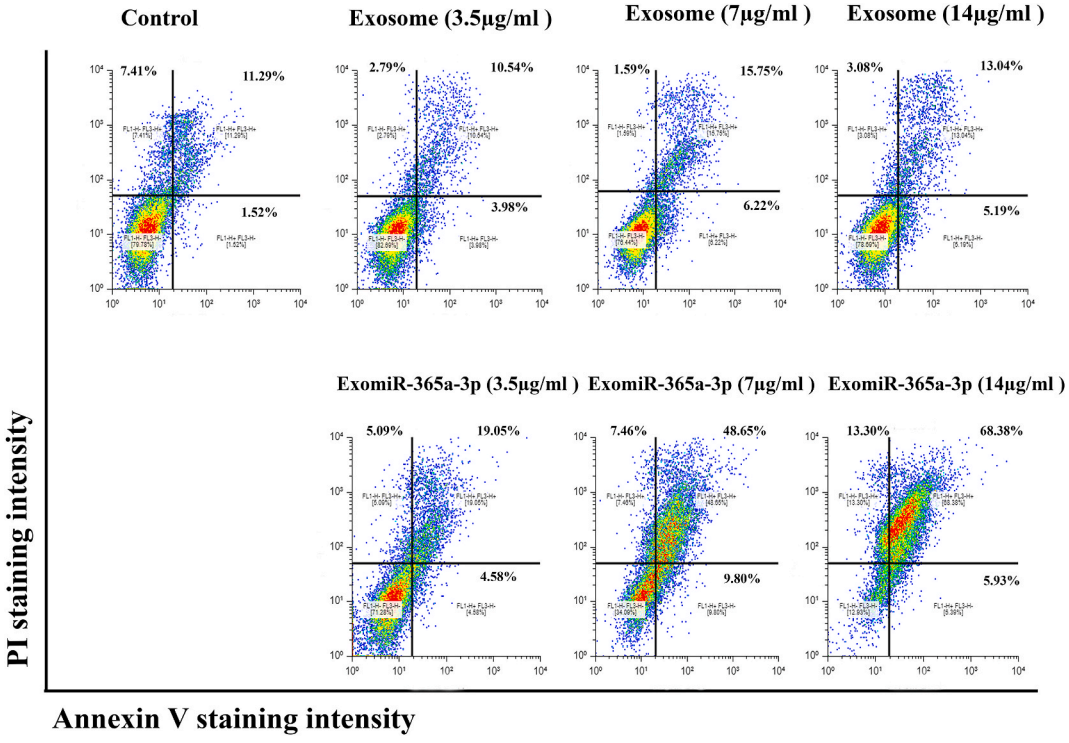

Fig. 4. Flow cytometry quantitative analysis of apoptotic cells. Dot blots showing the late and early apoptotic cells in HepG2 cell line 48 h after treatment with exosomes and ExomiR-365a-3p in different concentrations (3.5, 7, and 14 μg/ml) stained by Annexin V/PI.

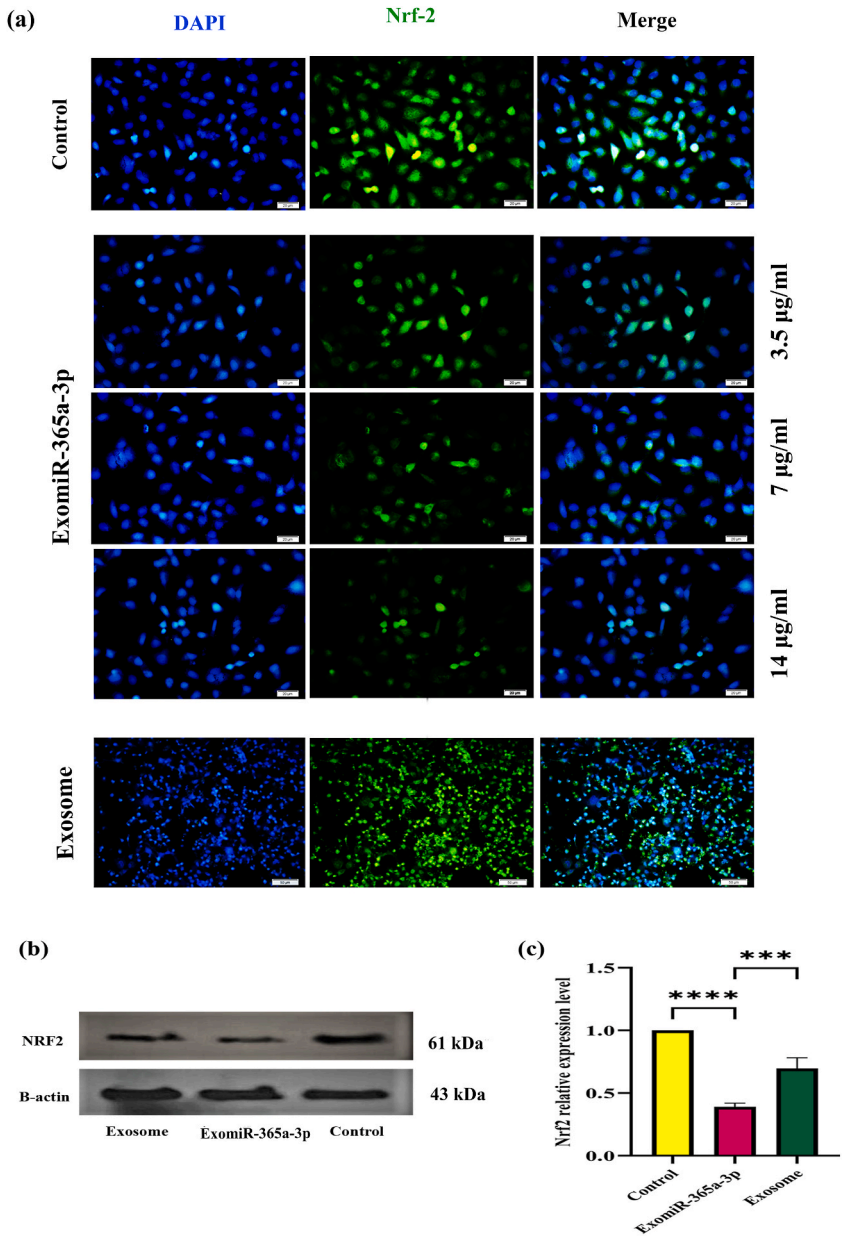

Fig. 5. The level of Nrf2 is increased in HCC and downregulated by ExomiR-365a-3p. (a) Localization and levels of Nrf2 were determined through immunocytochemistry using an anti-Nrf2 antibody (green fluorescence), DAPI was used to identify cell nuclei localization, (blue, center panel). The microscopic images demonstrate that ExomiR-365a-3p downregulates Nrf2 levels in a dose-dependent manner. (b) Western blot was performed to analyze the level of Nrf2 protein. The blot analysis showed that Nrf2 protein expression is downregulated in the group treated with ExomiR-365a-3p for 48 h, The original gel blot is shown in Fig. 5b of the Supplementary file. (c) According to the graph, the ExomiR-365a-3p-treated group showed a dramatic decrease in Nrf2 protein level. (All data are presented as the mean ± SD of three independent experiments. ****p-value <0.0001. One-way ANOVA was used to make comparisons between groups. (For interpretation of the references to color in this figure legend, the reader is referred to the Web version of this article.)

the treatment groups. To investigate the potential contribution of miR-365a-3p-enriched exosomes to increasing the ROS levels, a fluorogenic dye (DCFDA) was used to detect intracellular ROS. The results showed that Nrf2 suppression through ExomiR-365a-3p led to a dose-dependent elevation of ROS compared to the untreated and unloaded exosome groups (Fig. 7a and b) (p-value<0.0001).

Bcl-2, a direct target of miR-365a-3p, plays a crucial role in promoting cellular survival and inhibiting the actions of pro-apoptotic proteins. The effects of ExomiR-365a-3p on *Bcl*-2 mRNA levels were assessed by qRT-PCR (Fig. 7c). The qRT-PCR analysis revealed a significant downregulation of *Bcl*-2 mRNA expression and anti-apoptotic mRNA in HepG2 cells treated with exomiR-365a-3p compared to the exosome-treated and control groups (p-value<0.0001) and (p-value = 0.0001), However, no significant difference

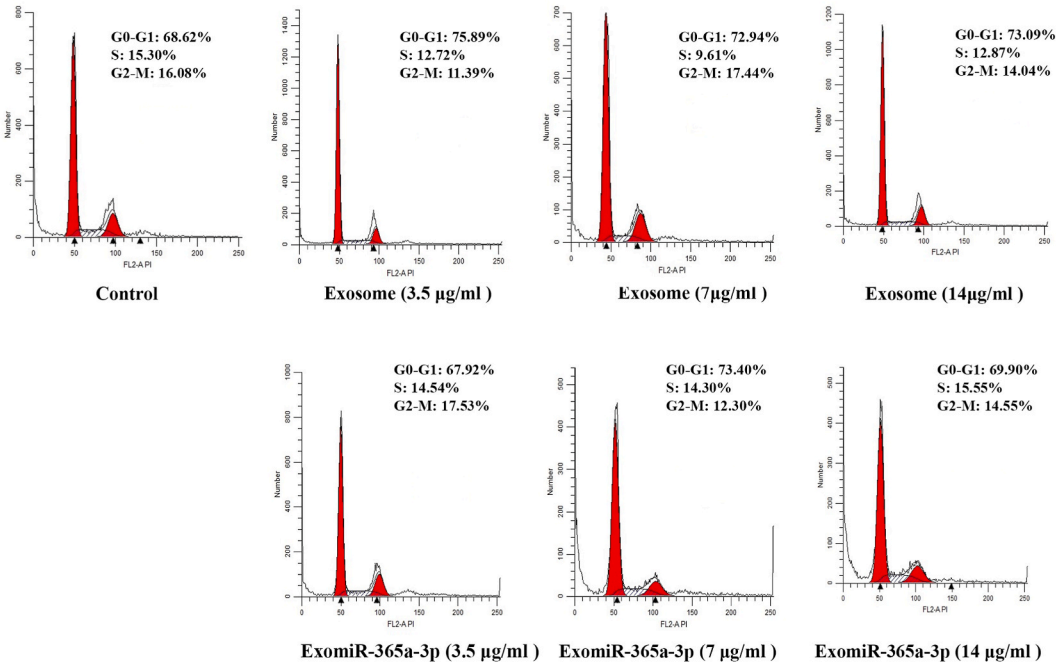

Fig. 6. The influence of ExomiR-365a-3p mimic on cell cycle distribution of HepG2 cells. The flow cytometry histograms of control (non-treated cells), exsosome treated cells (doses: 3.5, 7, 14 µg/ml), ExomiR-365a-3p mimic-treated cell (doses:3.5, 7, 14 µg/ml). The graphs show disorganization of cell cycle, an increase in sub G phase cells (apoptotic cells), and an increase in cell population at G0/G1 after exosome and ExomiR-365a treatments.

was observed between the exosome-treated groups and the control group (Fig. 7c).

3.8. ExomiR-365a-3p mimic reduces HepG2 in vitro migration and metastasis

The scratch wound healing test as an *in vitro* model of migration/metastasis along with western blotting for the ADAM10 protein was used to evaluate the impact of ExomiR-365a-3p on the metastasis and migration ability of HepG2 cells. The findings revealed a significant reduction in cell movement and migration in the ExomiR-365a-3p group after 24 h and 48 h compared to the exosomes and control groups. The gap in the scratch remained unfilled for 48 h (Fig. 8a), while the scratched wounds in the non-treated and exosome-treated cells were healed. The levels of ADAM10 protein, known to promote migration and invasion were determined by Western blotting (Fig. 8b and c). The ExomiR-365a-3p treatment resulted in a decrease in ADAM10 expression in HepG2 compared to the exosome-treated and control groups.

3.9. Model figure of the study and effects of ExomiR-365a on HepG2

Gao et al. demonstrated that miR-365 can directly bind to the 3′UTR region of Nrf2 mRNA and negatively regulate its expression [31]. Additionally, Nrf2 is a protein that is actively involved in cytoprotection mechanisms [32]. Due to accelerated cancer cell proliferation cycles, higher levels of ROS are common, and cells adapt themselves by increasing their antioxidant capacity to reduce ROS and prevent its accumulation, which can lead to senescence and apoptosis [9].

Based on these findings, our research hypothesized that inhibition of cytoprotective Nrf2 through miR-365a-3p as its regulator may induce apoptosis and other anti-tumor effects. Our results confirmed the mentioned negative effects of miR-365a-3p and, utilizing exosomes derived from HEK293 for miR-365a delivery, revealed additional synergistic anti-cancer effects. The work flow and the effects of ExomiR are depicted schematically in Fig. 9.

4. Discussion

Treatment of HCC is extremely challenging and requires a comprehensive understanding of the mechanisms involved in its pathogenesis. MicroRNAs mediate post-transcriptional gene regulation in cells, targeting mRNA activity in cellular processes [28]. These processes are vital for keeping cancer cells protected, in particular, against oxidative damage [29]. MiR-365a-3p has been reported as substantially downregulated in breast, gastric, and HCC cancers [33,34]. Delivering naked miRNA to target tissue is difficult due to endosomal entrapment, enzymatic degradation in body fluids, and immune surveillance [35–40]. Therefore, using proper carriers can enhance the stability, permeability, and efficiency of tumor suppressor microRNA transfection. Recent reports have

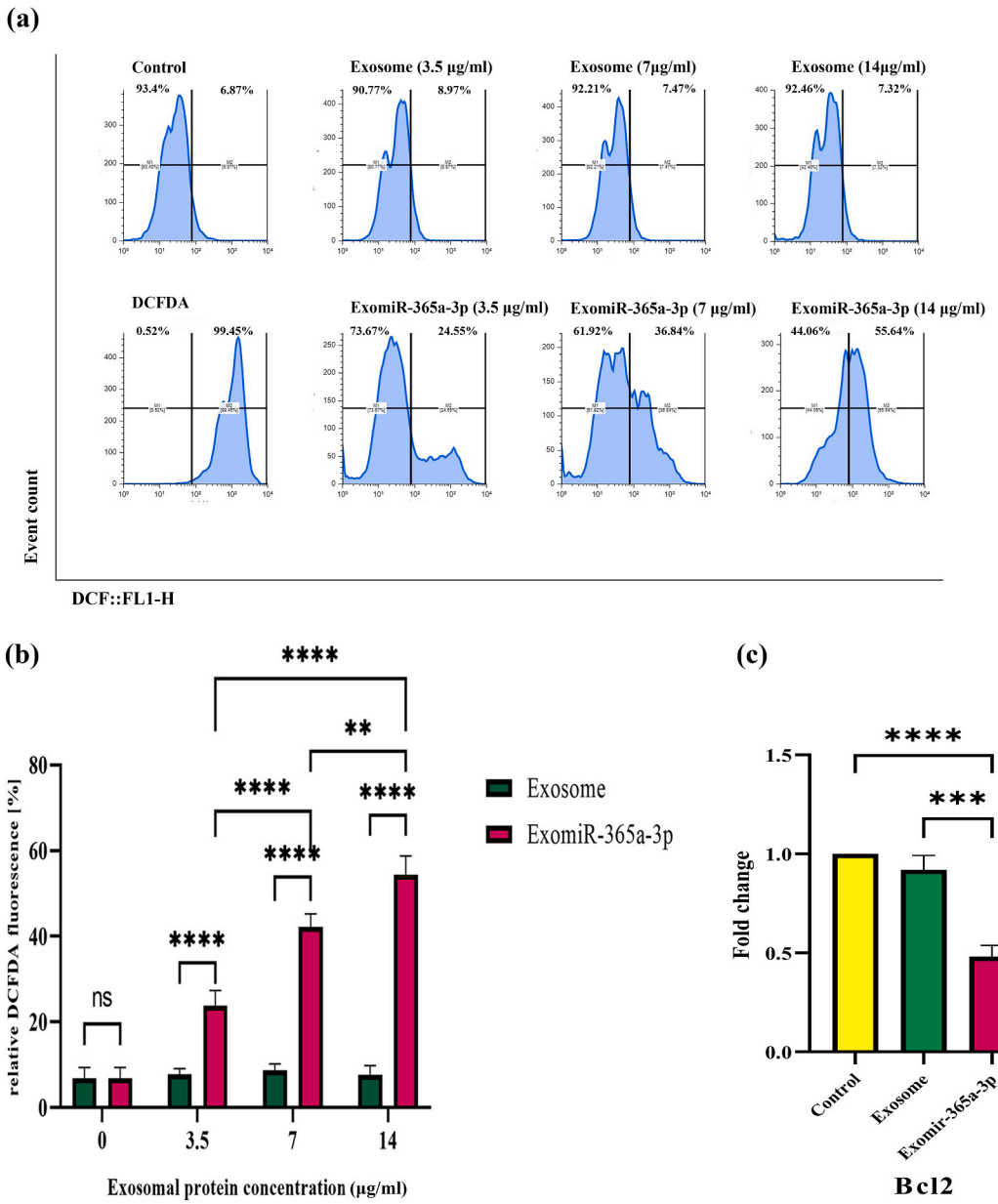

Fig. 7. Flow cytometry analysis of ROS generation and *Bcl-2* gene relative expression (a). ROS detected by DCFDA staining. Increased level of ROS is indicated in the groups treated with ExomiR-365a-3p in a dose-dependent manner. As compared to control groups, no significant changes of fluorescence were observed in the groups treated with different concentrations of exosomes. (b) Spectrophotometric fluorescence intensity measurement, which indicates a significant difference between the groups treated with exosomes and those treated with ExomiR-365a-3p (p-value< 0.0001). (c) The relative expression of *Bcl-2* in HepG2 cells treated with unloaded and miR-365a-3p-loaded HEK293-derived exosomes determined by qRT-PCR. Downregulation of the expression of *Bcl-2* was verified in HepG2 cells treated with ExomiR-365a-3p.. (All data are presented as the mean ± SD of three independent experiments ****p-value< 0.0001. One-way ANOVA was used to make comparisons between groups.)

emphasized the efficiency and biological origin of exosomes; thus, they can be employed in RNAi delivery [41]. To the best of our knowledge, there is no report about the application of HEK293-derived ExomiR-365a-3p against the HepG2 cell line.

The HEK293-derived exosomes showed proper size, morphology, miRNA carrying, and potential anti-tumor functions. Previous studies have reported that, these exosomes have several advantages over other sources for RNAi delivery. For instance, cancer cell-derived exosomes were active and could interfere with study results by promoting undesirable tumor activation and metastasis [25,42,43]. In agreement with the results of the present study, Zhu et al. stated that HEK293-derived exosomes were nontoxic and showed no significant adverse effects on mice [43]. Furthermore, HEK293-derived exosomes may possess similar membrane properties to tissues including the liver, brain, and skin. These characteristics suggest that HEK293-derived exosomes are likely to facilitate

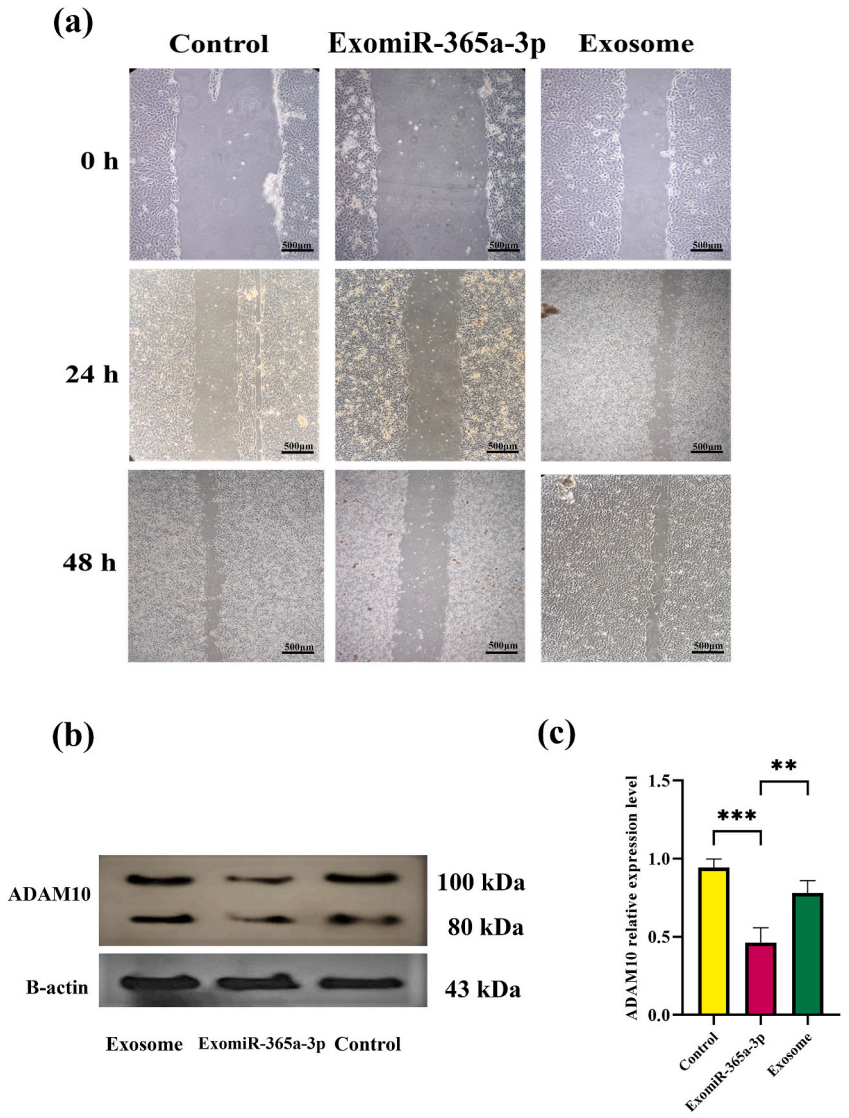

Fig. 8. Cell migration assay was performed by wound healing assay. (a) The images demonstrate that cell migration into the cell-free region was significantly decreased in the presence of 14 μg/m ExomiR-365a-3p when compared to exosome-treated and control groups. (b) Over-expression of ADAM10 promoted migration and invasion in HepG2 cells. Western blot analyzed the ADAM10 expression in three different groups. The original gel blot of ADAM10 and β-actin are shown in Figs. 8b and 5b of the Supplementary file (c) The analyzed data demonstrate that ExomiR-365a-3p lessened the level of ADAM10 considerably. All data are presented as the mean ± SD of three independent experiments. ***p*-value <0.001 and ****p*–value <0.0001. One-way ANOVA was used to make comparisons between groups.

well-organized membrane fusion with cells in these tissues. No studies have investigated the effects of cell line-produced self-exosomes and exosomes of other origins, such as HEK293. In the present study, we used HEK293-derived exosomes. Of course, HepG2 cells may secrete their own exosomes and signaling properties, but there is no significant difference between the results of the control routine medium group and the HEK293-derived exosome-treated group in our tests. It can be said that this possible interaction had no interference with our study. Future studies regarding interactions between cancer cell derived exosomes and therapeutic exogenous exosomes could be very interesting and may help more accurately design anti-cancer strategies.

The functions of hsa-miR-365a-3p have been reported to differ depending on tissues/disease type and genetic backgrounds, wherein it was documented to play either tumor suppressor or oncogene roles [44]. For instance, hsa-miR-365a promotes lung and laryngeal carcinogenesis [45,46], but in contrast, it suppresses cancer progression in colon and melanoma cancer [47,48].

The dual roles of hsa-miR-365a-3p in different contexts may be linked to its topological structure or the presence of multiple targets, enabling it to interact with active mRNAs in various signaling pathways and, subsequently, influencing of different cellular processes.

Based on our experimental phase results, we speculated that hsa-miR-365a-3p may suppress tumorigenesis in HCC. Our findings

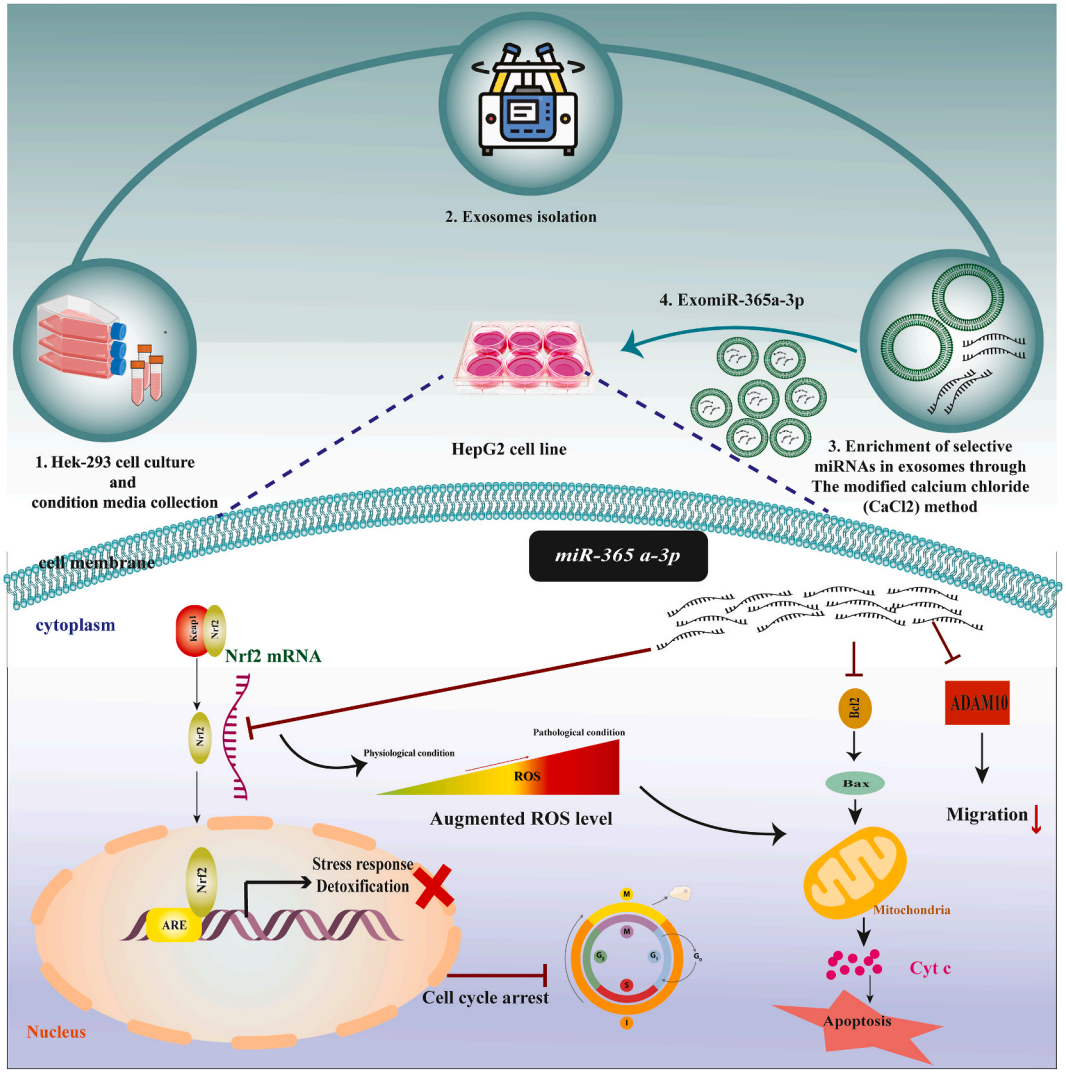

Fig. 9. Schematic general workflow of the study and effects of ExomiR-365 on HepG2 cells. miR-365 is a microRNA implicated in various cellular process and is known to target multiple genes. It has also been shown to directly target *Nrf2* and inhibit its expression. This can lead to a decrease in the antioxidant defense system and an increase in oxidative stress, potentially triggering apoptosis. Moreover, it has been found that miR-365 downregulates *Bcl2* expression, promoting apoptosis by reducing its anti-apoptotic activity. miR-365-mediated regulation of *Nrf2* and *bcl2* can potentially impact cell cycle progression and lead to dysregulation of the cell cycle. In addition, miR-365 directly targets the 3′UTR region of *ADAM1*0 mRNA and suppresses its expression.

were in line with those of Nei et al., Gastaldi et al., and others [47–49]. The discrepancies among miR-365a-focused studies may be attributed to the dynamic nature of each tumor microenvironment, the tumor progression stage, or the various signaling pathway types of cancers investigated [48].

The miRNAs presenting tumor suppressive properties can negatively affect the cell division cycle and induce arrest by targeting some cell cycle machinery mRNAs [50]. ExomiR-365a-3p transfection resulted in the perturbation of the ratio of populations in G0/G1, S, and G2/M phases compared to the HepG2 cells exposed to routine media. Hence, ExomiR-365a-3p can change the cell cycle balance in favor of the extinction of cancer cells. Moreover, the entry of the ExomiR-365a-3p into HepG2 cells augmented ROS levels. The elevated amounts of ROS could lead to apoptosis, probably because of a decline in ROS tuning mechanisms, particularly Nrf2 protein mediated functions. Over-expression of Nrf2 has a pivotal role in hepatoma growth and chemo-resistance by antioxidant mechanisms [51]. As described in the introduction section, rapid proliferation cycles of tumor cells, may occur together with the accumulation of higher ROS levels. Therefore, cells try to adapt by intensifying their antioxidant capacity to reduce ROS and prevent its augmentations, which can prompt senescence and apoptosis [9]. Nrf2 is an important cytoprotective protein. Over-activation of Nrf2 induces growth and enhances resistance to chemotherapy and metastasis through drug detoxification, inhibition of drug accumulation via drug efflux transporters, and the prevention of apoptosis [13]. Nrf2 activation has been demonstrated to boost cellular antioxidant capacity and control ROS levels, which can contribute to the reduction in apoptotic cell death. The current results showed that the downregulation

of Nrf2 using hsa-miR-365a increased ROS levels and subsequently disturbed the cell cycle and caused apoptotic cell death.

The current study verified the findings of previous research regarding the negative effects of miR-365a-3p on Nrf2 protein [52]. Other papers have revealed that miRNAs are able to regulate redox homeostasis and cytoprotection mechanisms with subsequent apoptosis promotion [53–55].

Additionally, an increase in the population of apoptotic cells and the downregulation of *Bcl2* mRNAs were detected in ExomiR-365a-3p-exposed cells. In agreement with the current work, targeting of the same *Bcl2* and *cyclin D1* mRNA was performed in melanoma cells by miR-365 treatment [47]. The current findings confirmed those of earlier investigations concerning a direct correlation between miR-365a-3p elevation and function in cells and cell suicide promotion. In addition, cells treated with ExomiR-365a-3p showed a series of behavioral changes, such as inhibition of cell migration in scratch wound healing assay. ADAM10 is known as an ADAM protein family member, and when it becomes upregulated, result in enhanced cell growth, cancer cell migration, and invasion [56,57]. Furthermore, activation of Nrf2 signaling enhance the expression of the two proteins, ADAM10 and ADAM17 [58]. Our findings are in agreement with the study of Yuan et al., which showed that specifically targeting ADAM10 expression with siRNA led to a significant decrease in the migration of HepG2 cells [59].

Considering the mentioned points, we analyzed the ADAM10 protein level and wound healing process. Our data demonstrated that Nrf2 downregulation could induce ADAM10 negative regulation with subsequent migration inhibition. The data are in line with reports by Fei Liu et al. [56] and confirm the anti-migration (metastasis) induction of ExomiR-365a-3p *in vitro*.

The current study has several limitations. First, it focused on a single model cell line (HepG2), which may not fully represent the complexity of HCC in clinical settings. Further studies using diverse HCC cell lines and primary tumor samples are needed for validation. Additional functional assays and *in vivo* models are required to evaluate the overall therapeutic potential and efficacy of ExomiR-365a-3p in the treatment of HCC. Moreover, future investigations could aim to evaluate off-target effects of ExomiR-365a-3p, its interaction with other pathways, and its long-term safety profile and biodistribution. Finally, exosomes could be engineered to help active targeting of HCC.

The discovery of microRNAs having the potential for negative regulation of oxidative stress defense provides an innovative strategy to exclusively overcome ROS-mediated cancer development and benefit from ROS-activated apoptosis. The findings of the current study may help in the development of efficient biotherapies against HCC through restoration of hsa-miR-365a.

5. Conclusion

In conclusion, when HEK293-derived exosomes are loaded with an miR-365a-3p mimic, they can restore the tumor suppressor miRNA levels in HepG2 cells. They diminish Nrf2 protein levels, disturb cell cycle progression, induce high ROS-mediated stress, enhance apoptosis rate, and reduce migration behavior by affecting ADAM10 in HepG2 cells. ExomiR-365a-3p mimic can be a robust biotherapeutic to generate an efficient anti-HCC strategy at post-transcriptional levels possibly using inhibition of the cytoprotection mechanism.

Ethics approval

Ethics code: IR.TBZMED.VCR.REC.1400.144.

Availability of data and material

All data obtained or analyzed in the present study are included in the manuscript and its Supplementary Information.

Funding

The present study was funded by the Deputy for Research and Technology, Faculty of Advanced Medical Sciences, Tabriz University of Medical Sciences under grant number 66583.

Data availability statement

Data will be made available on request.

CRediT authorship contribution statement

Armita Ghotaslou: Writing – original draft, Visualization, Software, Resources, Project administration, Methodology, Investigation, Formal analysis, Data curation. **Arezou Azizsoltani:** Writing – original draft, Validation, Software, Resources, Project administration, Methodology, Investigation, Formal analysis, Data curation. **Kaveh Baghaei:** Writing – original draft, Visualization, Supervision, Software, Methodology, Data curation. **Effat Alizadeh:** Writing – review & editing, Writing – original draft, Validation, Supervision, Investigation, Formal analysis, Data curation, Conceptualization.

Declaration of competing interest

The authors declare that they have no known competing financial interests or personal relationships that could have appeared to influence the work reported in this paper.

Acknowledgments

The authors would like to thank the Deputy for Research and Technology, Faculty of Advanced Medical Sciences, Tabriz University of Medical Sciences, Iran, for their financial support; grant number: 66583, ethics code: IR.TBZMED.VCR.REC.1400.144.

Appendix A. Supplementary data

Supplementary data to this article can be found online at https://doi.org/10.1016/j.heliyon.2024.e29333.

References

[1] P.H. Nguyen, S. Ma, C.Z. Phua, N.A. Kaya, H.L. Lai, C.J. Lim, J.Q. Lim, M. Wasser, L. Lai, W.L. Tam, Intratumoural immune heterogeneity as a hallmark of tumour evolution and progression in hepatocellular carcinoma, Nat. Commun. 12 (1) (2021) 1–13.
[2] Q.M. Anstee, H.L. Reeves, E. Kotsiliti, O. Govaere, M. Heikenwalder, From NASH to HCC: current concepts and future challenges, Nat. Rev. Gastroenterol. Hepatol. 16 (7) (2019) 411–428.
[3] X. Luo, S. Shen, S. Yi, J. Hu, Y. Sun, K. Gao, L. Zhu, Screening of differentially expressed miRNAs in tensile strain-treated HepG2 cells by miRNA microarray analysis, Mol. Med. Rep. 21 (6) (2020) 2415–2426.
[4] K. Otmani, P. Lewalle, Tumor suppressor miRNA in cancer cells and the tumor microenvironment: mechanism of deregulation and clinical implications, Front. Oncol. (2021) 4208.
[5] R. Yang, G. Liu, L. Han, Y. Qiu, L. Wang, M. Wang, MiR-365a-3p-mediated regulation of HELLS/GLUT1 axis suppresses aerobic glycolysis and gastric cancer growth, Front. Oncol. 11 (2021) 616390.
[6] Z. Chen, H. Xie, M. Hu, T. Huang, Y. Hu, N. Sang, Y. Zhao, Recent progress in treatment of hepatocellular carcinoma, Am. J. Cancer Res. 10 (9) (2020) 2993.
[7] C.R. Reczek, N.S. Chandel, The Two Faces of Reactive Oxygen Species in Cancer, 2017.
[8] Q. Zhang, W. Chen, X. Lv, Q. Weng, M. Chen, R. Cui, G. Liang, J. Ji, Piperlongumine, a novel TrxR1 inhibitor, induces apoptosis in hepatocellular carcinoma cells by ROS-mediated ER stress, Front. Pharmacol. 10 (2019) 1180.
[9] M. Dodson, R. Castro-Portuguez, D.D. Zhang, NRF2 plays a critical role in mitigating lipid peroxidation and ferroptosis, Redox Biol. 23 (2019) 101107.
[10] L. Lignitto, S.E. LeBoeuf, H. Homer, S. Jiang, M. Askenazi, T.R. Karakousi, H.I. Pass, A.J. Bhutkar, A. Tsirigos, B. Ueberheide, Nrf2 activation promotes lung cancer metastasis by inhibiting the degradation of Bach1, Cell 178 (2) (2019) 316–329. e18.
[11] D. Tseeleesuren, H.-H. Hsiao, R. Kant, Y.-C. Huang, H.-P. Tu, C.-C. Lai, S.-F. Huang, C.-H. Yen, The expression and prognostic value of cancer stem cell markers, NRF2, and its target genes in TAE/TACE-treated hepatocellular carcinoma, Medicina 58 (2) (2022) 212.
[12] H. Satoh, T. Moriguchi, J. Takai, M. Ebina, M. Yamamoto, Nrf2 prevents initiation but accelerates progression through the kras signaling pathway during lung CarcinogenesisNrf2 in kras-mutant lung cancer, Cancer Res. 73 (13) (2013) 4158–4168.
[13] S. Wu, H. Lu, Y. Bai, Nrf2 in cancers: a double-edged sword, Cancer Med. 8 (5) (2019) 2252–2267.
[14] C. Zhang, L. Shu, A.-N.T. Kong, MicroRNAs: new players in cancer prevention targeting Nrf2, oxidative stress and inflammatory pathways, Current pharmacology reports 1 (1) (2015) 21–30.
[15] M. Mullooly, P.M. McGowan, S.A. Kennedy, S.F. Madden, J. Crown, N. O' Donovan, M.J. Duffy, ADAM10: a new player in breast cancer progression? Br. J. Cancer 113 (6) (2015) 945–951.
[16] N. Gavert, M. Sheffer, S. Raveh, S. Spaderna, M. Shtutman, T. Brabletz, F. Barany, P. Paty, D. Notterman, E. Domany, Expression of L1-CAM and ADAM10 in human colon cancer cells induces metastasis, Cancer Res. 67 (16) (2007) 7703–7712.
[17] T. Knösel, A. Emde, K. Schlüns, Y. Chen, K. Jürchott, M. Krause, M. Dietel, I. Petersen, Immunoprofiles of 11 biomarkers using tissue microarrays identify prognostic subgroups in colorectal cancer, Neoplasia 7 (8) (2005) 741–747.
[18] Y.G. Hong, C. Xin, H. Zheng, Z.P. Huang, Y. Yang, J.D. Zhou, X.H. Gao, L. Hao, Q.Z. Liu, W. Zhang, L.Q. Hao, miR-365a-3p regulates ADAM10-JAK-STAT signaling to suppress the growth and metastasis of colorectal cancer cells, J. Cancer 11 (12) (2020) 3634–3644.
[19] Y. Chen, D.-Y. Gao, L. Huang, In vivo delivery of miRNAs for cancer therapy: challenges and strategies, Adv. Drug Deliv. Rev. 81 (2015) 128–141.
[20] D. Liang, C. Liu, M. Yang, Mesenchymal stem cells and their derived exosomes for ALI/ARDS: a promising therapy, Heliyon 9 (10) (2023) E20387.
[21] X. Lv, Z. Li, Y. Dai, Y. Xiao, F. Shen, J. Wang, J. Cao, L. Wang, Q. Peng, Y. Jiao, The mir-199b-5p encapsulated in adipocyte-derived exosomes mediates radioresistance of colorectal cancer cells by targeting JAG1, Heliyon 10 (2) (2024) e24412.
[22] I.-Y. Kim, H.Y. Kim, H.-w. Song, J.-O. Park, Y.H. Choi, E. Choi, Functional enhancement of exosomes derived from NK cells by IL-15 and IL-21 synergy against hepatocellular carcinoma cells: the cytotoxicity and apoptosis in vitro study, Heliyon 9 (6) (2023) e16962.
[23] A. Azizsoltani, B. Hatami, M.R. Zali, V. Mahdavi, K. Baghaei, E. Alizadeh, Obeticholic acid-loaded exosomes attenuate liver fibrosis through dual targeting of the FXR signaling pathway and ECM remodeling, Biomed. Pharmacother. 168 (2023) 115777.
[24] D. Lopes, J. Lopes, M. Pereira-Silva, D. Peixoto, N. Rabiee, F. Veiga, O. Moradi, Z.H. Guo, X.D. Wang, J. Conde, Exosomal-Membrane-Camouflaged Abiotic Nanocarriers: Neurodegenerative Diseases, Tissue Engineering and Regenerative Medicine, 2023.
[25] X. Zhu, M. Badawi, S. Pomeroy, D.S. Sutaria, Z. Xie, A. Baek, J. Jiang, O.A. Elgamal, X. Mo, K.L. Perle, Comprehensive toxicity and immunogenicity studies reveal minimal effects in mice following sustained dosing of extracellular vesicles derived from HEK293T cells, J. Extracell. Vesicles 6 (1) (2017) 1324730.
[26] S. Ferguson, S. Kim, C. Lee, M. Deci, J. Nguyen, The phenotypic effects of exosomes secreted from distinct cellular sources: a comparative study based on miRNA composition, AAPS J. 20 (4) (2018) 1–13.
[27] M. Khalili, A. Zarebkohan, H. Dianat-Moghadam, M. Panahi, H. Andre, E. Alizadeh, Corneal endothelial cell sheet bioengineering from neural crest cell-derived adipose stem cells on novel thermo-responsive elastin-mimetic dendrimers decorated with RGD, Chem. Eng. J. 429 (2022) 132523.
[28] P. Briata, R. Gherzi, Long non-coding RNA-ribonucleoprotein networks in the post-transcriptional control of gene expression, Non-coding RNA 6 (3) (2020) 40.
[29] A. Forterre, H. Komuro, S. Aminova, M. Harada, A comprehensive review of cancer MicroRNA therapeutic delivery strategies, Cancers 12 (7) (2020) 1852.
[30] E. Akbari, H. Mousazadeh, Z. Sabet, T. Fattahi, A. Dehnad, A. Akbarzadeh, E. Alizadeh, Dual drug delivery of trapoxin A and methotrexate from biocompatible PLGA-PEG polymeric nanoparticles enhanced antitumor activity in breast cancer cell line, J. Drug Deliv. Sci. Technol. 61 (2021) 102294.
[31] M. Gao, C. Li, M. Xu, Y. Liu, M. Cong, S. Liu, LncRNA MT1DP aggravates cadmium-induced oxidative stress by repressing the function of Nrf2 and is dependent on interaction with miR-365, Adv. Sci. 5 (7) (2018) 1800087.
[32] S. Ghareghomi, M. Habibi-Rezaei, M. Arese, L. Saso, A.A. Moosavi-Movahedi, Nrf2 modulation in breast cancer, Biomedicines 10 (10) (2022) 2668.

[33] D. Hong, A. Zang, Z. Wang, L. Yang, G. Ren, C. Zhang, L. Zhang, W. Hou, Y. Wei, Elevation of microRNA-365 impedes malignant behaviors of gastric cancer cells by inhibiting PAX6, Funct. Integr. Genom. 22 (5) (2022) 825–834.
[34] Z. Chen, Z. Huang, Q. Ye, Y. Ming, S. Zhang, Y. Zhao, L. Liu, Q. Wang, K. Cheng, Prognostic significance and anti-proliferation effect of microRNA-365 in hepatocellular carcinoma, Int. J. Clin. Exp. Pathol. 8 (2) (2015) 1705.
[35] G. Kara, G.A. Calin, B. Ozpolat, RNAi-based therapeutics and tumor targeted delivery in cancer, Adv. Drug Deliv. Rev. (2022) 114113.
[36] L. Wu, W. Zhou, L. Lin, A. Chen, J. Feng, X. Qu, H. Zhang, J. Yue, Delivery of therapeutic oligonucleotides in nanoscale, Bioact. Mater. 7 (2022) 292–323.
[37] C. Zhao, X. Sun, L. Li, Biogenesis and function of extracellular miRNAs, ExRNA 1 (1) (2019) 1–9.
[38] C.V. Pecot, G.A. Calin, R.L. Coleman, G. Lopez-Berestein, A.K. Sood, RNA interference in the clinic: challenges and future directions, Nat. Rev. Cancer 11 (1) (2011) 59–67.
[39] C.S. Gondi, J.S. Rao, Concepts in in vivo siRNA delivery for cancer therapy, J. Cell. Physiol. 220 (2) (2009) 285–291.
[40] H. Qin, Y. Ji, G. Li, X. Xu, C. Zhang, W. Zhong, S. Xu, Y. Yin, J. Song, MicroRNA-29b/graphene oxide–polyethyleneglycol–polyethylenimine complex incorporated within chitosan hydrogel promotes osteogenesis, Front. Chem. 10 (2022).
[41] D.S. Sutaria, J. Jiang, O.A. Elgamal, S.M. Pomeroy, M. Badawi, X. Zhu, R. Pavlovicz, A.C.P. Azevedo-Pouly, J. Chalmers, C. Li, Low active loading of cargo into engineered extracellular vesicles results in inefficient miRNA mimic delivery, J. Extracell. Vesicles 6 (1) (2017) 1333882.
[42] G.B. Kim, G.-H. Nam, Y. Hong, J. Woo, Y. Cho, I.C. Kwon, Y. Yang, I.-S. Kim, Xenogenization of tumor cells by fusogenic exosomes in tumor microenvironment ignites and propagates antitumor immunity, Sci. Adv. 6 (27) (2020) eaaz2083.
[43] Y. Hong, G.H. Nam, E. Koh, S. Jeon, G.B. Kim, C. Jeong, D.H. Kim, Y. Yang, I.S. Kim, Exosome as a vehicle for delivery of membrane protein therapeutics, PH20, for enhanced tumor penetration and antitumor efficacy, Adv. Funct. Mater. 28 (5) (2018) 1703074.
[44] M. Li, L. Liu, W. Zang, Y. Wang, Y. Du, X. Chen, P. Li, J. Li, G. Zhao, miR-365 overexpression promotes cell proliferation and invasion by targeting ADAMTS-1 in breast cancer, Int. J. Oncol. 47 (1) (2015) 296–302.
[45] Y. Wang, S. Zhang, H. Bao, S. Mu, B. Zhang, H. Ma, S. Ma, MicroRNA-365 promotes lung carcinogenesis by downregulating the USP33/SLIT2/ROBO1 signalling pathway, Cancer Cell Int. 18 (1) (2018) 1–14.
[46] J. Geng, Y. Liu, Y. Jin, J. Tai, J. Zhang, X. Xiao, P. Chu, Y. Yu, S.C. Wang, J. Lu, S. Han, J. Shi, Y. Guo, X. Ni, MicroRNA-365a-3p promotes tumor growth and metastasis in laryngeal squamous cell carcinoma, Oncol. Rep. 35 (4) (2016) 2017–2026.
[47] Y. Zhu, X. Wen, P. Zhao, MicroRNA-365 Inhibits Cell Growth and Promotes Apoptosis in Melanoma by Targeting BCL2 and Cyclin D1 (CCND1), Medical Science Monitor: International Medical Journal of Experimental and Clinical Research, vol. 24, 2018, p. 3679.
[48] J. Nie, L. Liu, W. Zheng, L. Chen, X. Wu, Y. Xu, X. Du, W. Han, microRNA-365, down-regulated in colon cancer, inhibits cell cycle progression and promotes apoptosis of colon cancer cells by probably targeting Cyclin D1 and Bcl-2, Carcinogenesis 33 (1) (2012) 220–225.
[49] C. Gastaldi, T. Bertero, N. Xu, I. Bourget-Ponzio, K. Lebrigand, S. Fourre, A. Popa, N. Cardot-Leccia, G. Meneguzzi, E. Sonkoly, miR-193b/365a cluster controls progression of epidermal squamous cell carcinoma, Carcinogenesis 35 (5) (2014) 1110–1120.
[50] M.J. Bueno, M. Malumbres, MicroRNAs and the cell cycle, Biochim. Biophys. Acta (BBA) - Mol. Basis Dis. 1812 (5) (2011) 592–601.
[51] H.K.C. Ngo, D.-H. Kim, Y.-N. Cha, H.-K. Na, Y.-J. Surh, Nrf2 mutagenic activation drives HepatocarcinogenesisNrf2 drives hepatocarcinogenesis, Cancer Res. 77 (18) (2017) 4797–4808.
[52] B.N. Chorley, M.R. Campbell, X. Wang, M. Karaca, D. Sambandan, F. Bangura, P. Xue, J. Pi, S.R. Kleeberger, D.A. Bell, Identification of novel NRF2-regulated genes by ChIP-Seq: influence on retinoid X receptor alpha, Nucleic Acids Res. 40 (15) (2012) 7416–7429.
[53] J. He, B.-H. Jiang, Interplay between reactive oxygen species and microRNAs in cancer, Current pharmacology reports 2 (2) (2016) 82–90.
[54] S.-Z. Li, Y.-Y. Hu, J. Zhao, Y.-B. Zhao, J.-D. Sun, Y.-f. Yang, C.-C. Ji, Z.-B. Liu, W.-D. Cao, Y. Qu, MicroRNA-34a induces apoptosis in the human glioma cell line, A172, through enhanced ROS production and NOX2 expression, Biochem. Biophys. Res. Commun. 444 (1) (2014) 6–12.
[55] A. Magenta, C. Cencioni, P. Fasanaro, G. Zaccagnini, S. Greco, G. Sarra-Ferraris, A. Antonini, F. Martelli, M. Capogrossi, miR-200c is upregulated by oxidative stress and induces endothelial cell apoptosis and senescence via ZEB1 inhibition, Cell Death Differ. 18 (10) (2011) 1628–1639.
[56] F. Liu, L. Zhuang, R. Wu, D. Li, miR-365 inhibits cell invasion and migration of triple negative breast cancer through ADAM10, J buon 24 (5) (2019) 1905–1912.
[57] J. Guo, L. He, P. Yuan, P. Wang, Y. Lu, F. Tong, Y. Wang, Y. Yin, J. Tian, J. Sun, ADAM10 overexpression in human non-small cell lung cancer correlates with cell migration and invasion through the activation of the Notch1 signaling pathway, Oncol. Rep. 28 (5) (2012) 1709–1718.
[58] S. Castro-Sánchez, Á.J. García-Yagüe, S. Kügler, I. Lastres-Becker, CX3CR1-deficient microglia shows impaired signalling of the transcription factor NRF2: implications in tauopathies, Redox Biol. 22 (2019) 101118.
[59] S. Yuan, S. Lei, S. Wu, ADAM10 is overexpressed in human hepatocellular carcinoma and contributes to the proliferation, invasion and migration of HepG2 cells, Oncol. Rep. 30 (4) (2013) 1715–1722.